Ice shelf water overflow and bottom water formation in the southern Weddell Sea

A. Foldvik,[1] T. Gammelsrød,[1] S. Østerhus,[1] E. Fahrbach,[2] G. Rohardt,[2] M. Schröder,[2] K. W. Nicholls,[3] L. Padman,[4] and R. A. Woodgate[5]

Received 17 June 2003; revised 5 October 2003; accepted 10 December 2003; published 17 February 2004.

[1] Cold shelf waters flowing out of the Filchner Depression in the southern Weddell Sea make a significant contribution to the production of Weddell Sea Bottom Water (WSBW), a precursor to Antarctic Bottom Water (AABW). We use all available current meter records from the region to calculate the flux of cold water (<−1.9°C) over the sill at the northern end of the Filchner Depression (1.6 ± 0.5 Sv), and to determine its fate. The estimated fluxes and mixing rates imply a rate of WSBW formation (referenced to −0.8°C) of 4.3 ± 1.4 Sv. We identify three pathways for the cold shelf waters to enter the deep Weddell Sea circulation. One path involves flow constrained to follow the shelf break. The other two paths are down the continental slope, resulting from the cold dense water being steered northward by prominent ridges that cross the continental slope near 36°W and 37°W. Mooring data indicate that the deep plumes can retain their core characteristics to depths greater than 2000 m. Probably aided by thermobaricity, the plume water at this depth can flow at a speed approaching 1 m s^{-1}, implying that the flow is occasionally supercritical. We postulate that such supercriticality acts to limit mixing between the plume and its environment. The transition from supercritical to slower, more uniform flow is associated with very efficient mixing, probably as a result of hydraulic jumps. *INDEX TERMS:* 4207 Oceanography: General: Arctic and Antarctic oceanography; 4568 Oceanography: Physical: Turbulence, diffusion, and mixing processes; 4512 Oceanography: Physical: Currents; 4594 Oceanography: Physical: Instruments and techniques; 4520 Oceanography: Physical: Eddies and mesoscale processes; *KEYWORDS:* bottom water formation, mixing processes, hydraulic jump, current meters, Ice Shelf Water

Citation: Foldvik, A., T. Gammelsrød, S. Østerhus, E. Fahrbach, G. Rohardt, M. Schröder, K. W. Nicholls, L. Padman, and R. A. Woodgate (2004), Ice shelf water overflow and bottom water formation in the southern Weddell Sea, *J. Geophys. Res.*, *109*, C02015, doi:10.1029/2003JC002008.

1. Introduction

[2] Cold, dense and oxygenated Antarctic Bottom Water (AABW) is one of the Antarctic's most important exports. Production of AABW is routinely cited as being one of the drivers of the global thermohaline circulation (GTHC) and its influence on the properties of the World Ocean is widely accepted. Understanding the mechanisms for the production of AABW, and any sensitivity in those mechanisms to past or future climate change, is therefore important if we are to understand the controls on the GTHC. More than half of the total flux of AABW is believed to have its origins in the Weddell Sea [*Orsi et al.*, 1999].

[3] In today's climatic regime the majority of AABW production begins with the formation of High Salinity Shelf Water (HSSW) in Antarctica's marginal seas. HSSW is a by-product of sea-ice formation over many of the broader portions of the Antarctic continental shelf. One of the acknowledged hot spots for the production of HSSW is the western and southern margin of the Weddell Sea (Figure 1). A combination of winds blowing from the Filchner-Ronne Ice Shelf and tidal divergence at its seaward boundary maintains latent heat polynyas along the ice front for most of the year [*Foldvik et al.*, 2001; *Renfrew et al.*, 2002]. Intense heat loss from these polynyas, and also through leads in the pack ice over the continental shelf to the north, results in high rates of sea-ice production and HSSW formation. There are various pathways by which the HSSW can arrive in the deep Weddell Sea as Weddell Sea Bottom Water (WSBW), the Weddell Sea's precursor to AABW. One such pathway involves circulation in the ocean cavity beneath Filchner-Ronne Ice Shelf [*Foldvik and Gammelsrød*, 1988; *Nicholls et al.*, 2001].

[4] Although HSSW has a temperature close to the freezing point at the surface (−1.9°C) the depression of the freezing point of seawater with an increase in pressure

[1]Geophysical Institute, University of Bergen, Bergen, Norway.
[2]Alfred-Wegener-Institut fur Polar und Meeresforschung, Bremerhaven, Germany.
[3]British Antarctic Survey, Cambridge, UK.
[4]Earth and Space Research, Seattle, Washington, USA.
[5]Applied Physics Laboratory, University of Washington, Seattle, Washington, USA.

0148-0227/04/2003JC002008$09.00

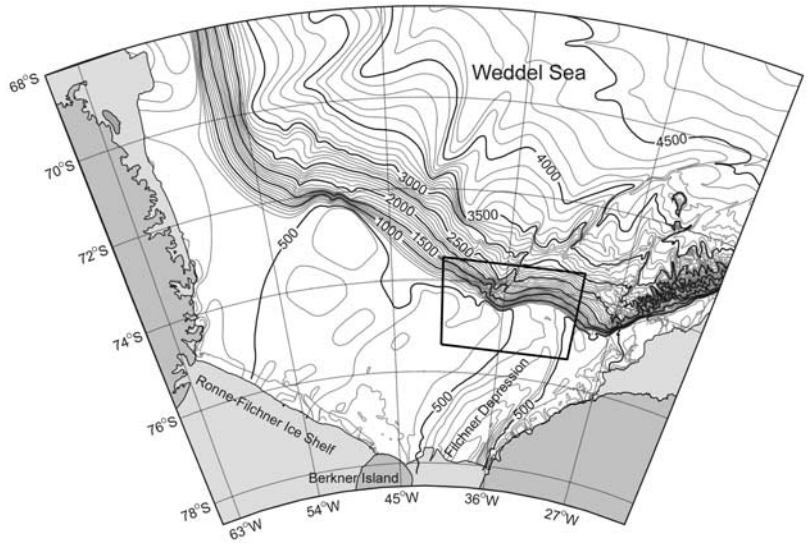

Figure 1a. Bathymetric map of the Weddell Sea with 100 m isobath intervals (data from GEBCO). The study area is indicated by a box.

means that, even at −1.9°C, HSSW retains the capacity to melt ice at depth. At the base of an ice shelf with a draft of 1500 m, for example, the freezing point is about −3.0°C [*Millero*, 1978], over a degree lower than the temperature of any HSSW that flows into the sub-ice shelf cavity. The interaction with the ice shelf causes HSSW to be cooled further and slightly diluted to form Ice Shelf Water (ISW, defined as water with potential temperature below its surface freezing point, ∼ −1.9°C), which is observed to flow out from beneath Filchner Ice Shelf at mid-water depths and at potential temperatures as low as −2.3°C [e.g., *Gammelsrød et al.*, 1994].

[5] The ISW that finally escapes the Filchner Depression (Figure 1) descends the continental slope north of Filchner Ice Shelf. Here cross-slope advection by high-frequency processes such as tides [*Middelton et al.*, 1987; *Foldvik et al.*, 1990] and shelf waves [*Middelton et al.*,1982] in addition to local wind conditions and the strength and location of the Antarctic Slope Front may determine whether the cold plumes remain near the shelf break or rapidly sink west of the sill. It will be shown that the fate of the cold plumes also depends on two prominent ridges that act to steer the flows toward the north, aided by the thermobaric effect [*Killworth*, 1977]. The cold plumes ultimately contribute to the formation of WSBW by mixing with overlying Weddell Deep Water (WDW).

[6] WSBW derived from ISW has properties that differ from WSBW formed with no direct participation of ice shelves [*Gordon*, 1998; *Mensch et al.*, 1998; *Schlosser et al.*, 1990]. The properties of the AABW ultimately formed from WSBW are therefore sensitive to the nature and volume flux of the ISW-derived component. Since the 1970s there have been several attempts to assess the contribution made by Filchner-Ronne ISW to the WSBW budget. Many recent mooring programs and cruises to the southern Weddell Sea have significantly increased the available data in this region.

[7] The primary purpose of the present study was to estimate the contribution of Filchner-Ronne ISW to WSBW production in the southern Weddell Sea, drawing on all available data. These data include hitherto unpublished time series of currents, temperature and salinity. The time series are up to 30 months in length and are from various moorings deployed over a 31-year period. In the following section we summarize the available data; in section 3 we describe the basic characteristics of the distribution of plumes of cold water in different years, and their fundamental characteristics of temperature and velocity. In section 4 we quantify the volume flux of cold water flowing out of the Filchner Depression, and in section 5 we use mixing relationships to estimate the associated production rate of WSBW. We conclude with a discussion and summary in section 6.

2. Data, Instruments and Methods

[8] We present results from 20 current meter moorings that have been deployed in the study area at various times

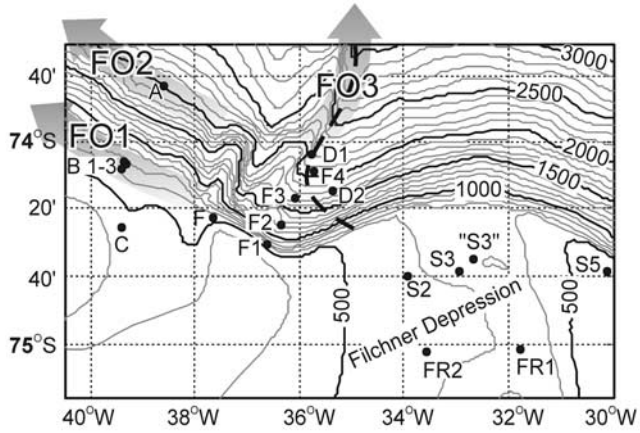

Figure 1b. Bathymetric map of the study area, including mooring names. The dashed line indicates the line of the CTD section shown in Figure 10. The shaded arrows indicate the pathways of cold shelf water identified in section 6.

Table 1. Current Meter Moorings Used in This Study[a]

Mooring Name	Deployed Year	Position		Bottom Depth, m	Deployment Vessel	Reference
		Lat.	Lon.			
B1	1968	−74 07	−39 18	657	Glacier	*Foldvik et al.* [1985b]
B2	1968	−74 08	−39 23	663		
B3	1977	−74 06	−39 22	600	Polarsirkel	*Foldvik et al.* [1985a]
C	1977	−74 26	−39 24	475		
S2	1977	−74 40	−33 56	558		
F	1977	−74 23	−37 39	470		
A	1978	−73 43	−38 36	1939	Glacier	*Middleton et al.* [1982]
D1	1985	−74 04	−35 45	2100	Andenes	*Nordlund* [1992]
D2	1985	−74 15	−35 22	1800		
S2	1985	−74 40	−33 56	545		
S3	1985	−74 39	−32 56	610		
S2	1987	−74 40	−34 00	558	Polarstern	*Østerhus and Krause* [1990]
S5	1990	−74 39	−30 07	450	Andenes	Unpublished data obtained 1990
"S3"	1992	−74 35	−32 39	659	Aurora	*Nygaard* [1994]
FR1	1995	−75 01	−31 46	610	Polarstern	*Woodgate et al.* [1998]
FR2	1995	−75 02	−33 33	574		
F1	1998	−74 31	−36 36	647	Endurance	*Fahrbach and El Naggar* [2001]
F2	1998	−74 25	−36 22	1180		
F3	1998	−74 17	−36 04	1637		
F4	1998	−74 09	−35 42	1984		

[a]Columns indicate the mooring name, year of deployment, position and bottom depth. The appropriate references are also shown.

between 1968 and 1999. The moorings are described in Table 1, and their locations shown in Figure 1. Note that moorings were deployed at position S2 on three different occasions. Aanderaa current meters (models RCM4, RCM5, RCM7 and RCM8) were used on the moorings, 44 instruments in total. The accuracy of the individual speed and direction measurements is ±1 cm s^{-1} and ±5°, respectively. Systematic errors may occur at very low speeds (<1cm s^{-1}), but as the speeds in the present time series are always well above this threshold level we assume errors from this source to be negligible. The observation depths, average velocity components and potential temperatures, together with their standard deviations, are given in Table 2.

[9] For the purpose of error estimates the RCM time series were de-tided and assumed to be first order autoregressive processes. The degrees of freedom (M) were determined by the time taken for the autocorrelation function to fall to $1/e$ (usually about 5 days). The standard error was obtained by dividing the standard deviations (Table 2) by $\sqrt{M}$. This error was then combined with other sources of error (width and height of plume) to produce the final error estimates for the transports.

[10] The F1–F4 moorings also carried Seabird MicroCAT (SBE-37) conductivity-temperature (CT) sensors at a height of 9 m above bottom (mab). The average results for those are given in Table 3. Tables 2 and 3 show that the MicroCAT temperature sensors agree well (0.04°C or better) with the temperature sensors mounted on current meters at the same positions on the moorings. The accuracy of the MicroCAT sensors is <0.01°C for temperature and <0.004 S m^{-1} for conductivity.

[11] The compass at the lowermost current meter at mooring F2 (10 mab) functioned for a 10-day period only. The average current values given in Table 2 are based on this period. During this 10-day period the directions given by the 10 mab instrument and the 56 mab instrument differed by only a few degrees at most. We have therefore reconstructed the 10 mab current vectors for the entire observation period using the observed speed together with the current direction from the 56 mab instrument above. It is this reconstructed record that is used in the transport calculations (section 4). If we assume that the error introduced by this procedure corresponds to the observed differences in direction between 10 mab and 56 mab at F1 then the error in the mean normal component 10 mab at F2 is at most 3%. At mooring F3 the current meter at 10 mab did not work at all. Assuming the same strong correlation between the currents at 10 mab and 56 mab for F3 as we see for F2, we synthesized the velocity at 10 mab on F3 from the F3 current meter record at 56 mab using linear regression. The temperature record from the F3 MicroCAT at 9 mab was used. We assume the error in the transport estimate from F3 at 10 mab to be similar to that from F2 at 10 mab, about 3%.

[12] The CTD temperatures presented here were obtained using a Neil Brown system in 1985 and 1990 on board "RV Andenes", and a Seabird system in 1999 on board "FS Polarstern". Typically the errors are within ±0.005°C.

[13] Throughout this paper salinities are measured on the Practical Salinity Scale 1978 [*United Nations Educational, Scientific and Cultural Organization* (*UNESCO*), 1981].

[14] The measurements presented here were obtained over a period of 30 years. It is therefore possible that direct comparison of the records might be compromised by interannual variability. For the most part we have assumed this part of the variability can be ignored, but we will discuss and justify this assumption in section 6.

3. Characteristics of the Filchner Overflow

3.1. Average Currents and Temperatures

[15] The average current velocities from the instruments on each mooring are shown in Figure 2 and Table 2. The deepest instruments are usually located at 10 mab or 25 mab (see Table 2). The average potential temperatures of the deepest instruments are also shown in Figure 2. Note that for several moorings near the sill of the Filchner Depression (the S and FR moorings) the average potential temperature is below the

Table 2. Summary of Current Meter Data[a]

Moor. name	Inst. Number	Depl. Year	Reco Days	Obs. Depth, m	mab, m	u, cm s^{-1}	ϕ_u, cm s^{-1}	v, cm s^{-1}	ϕ_v, cm s^{-1}	θ, °C	ϕ_θ, °C
B1	67	1968	265	634	23	−6.2	8.8	0.5	9.9	−1.05	0.33
B2	70	1968	460	640	23	−6.8	9.6	1.7	10.5	−0.95	0.25
B3	2393	1977	259	500	100	−6.0	7.5	1.6	8.3	−0.93	0.32
C	2391	1977	631	350	125	−3.3	4.8	2.2	5.2	−1.52	0.36
C	2390	1977	630	450	25	−3.3	4.3	2.5	4.5	−1.41	0.38
S2	2172	1977	257	458	100	−6.1	11	4.3	10	−1.93	0.34
S2	2174	1977	411	533	25	−5.7	8.9	5.4	8.3	−2.15	0.15
F	2388	1977	32	445	25	−19.6	18.5	4.9	22.3	−0.94	0.46
A	1360	1978	440	1814	125	−4.9	7.2	6	5.1	−1.25	0.14
A	1361	1978	65	1914	25	−7.7	5.8	5.5	5	−1.37	0.11
D1	7539	1985	352	2000	100	16.1	12	16.2	11.5	−0.63	0.44
D1	7540	1985	352	2075	25	27.2	14.6	24.4	12	−1.10	0.46
D2	7537	1985	52	1700	100	−6.1	9.1	−3.7	12	0.02	0.3
D2	7538	1985	281	1775	25	−15.7	16.8	−3.4	10.2	−0.47	0.63
S2	3160	1985	258	355	190	−3.6	9.9	2.4	10.2	−1.66	0.31
S2	4223	1985	283	445	100	−3.7	9.9	4.1	10.4	−1.96	0.17
S2	7716	1985	371	520	25	−4.8	9.4	6	9.7	−2.01	0.05
S3	3164	1985	212	510	100	−21.2	12.1	6.2	10.6	−1.92	0.25
S3	4277	1985	205	585	25	−23.5	11.8	7.4	9.7	−1.92	0.06
S2	8481	1987	407	459	100	−6.2	11.1	3.5	11.7	−2.02	0.17
S2	3160	1987	352	533	25	−4.6	9	4.2	9.4	−1.96	0.17
S5	39	1990	15	265	185	−0.2	3.5	0	4.1	−1.81	0.04
"S3"	3160	1992	356	489	170	−10.1	10.7	0.1	11.6	−1.44	0.38
"S3"	6796	1992	165	589	70	−12.0	12.5	−0.6	11	−1.92	0.33
FR1	10929	1995	828	257	353	−1.7	6	3.9	6.6	−1.80	0.22
FR1	10928	1995	828	378	232	−3.0	6.8	5.2	7.4	−2.00	0.09
FR1	9390	1995	837	484	126	−3.7	6.9	5.6	7.4	−2.03	0.04
FR1	1281	1995	691	590	20	−2.9	6.6	7	7.5	−2.05	0.03
FR2	10925	1995	829	191	383	3.0	7.3	−0.3	7.6	−1.78	0.12
FR2	10005	1995	829	342	232	1.5	6.6	−0.2	7	−1.88	0.22
FR2	9185	1995	837	448	126	0.7	6.4	0	6.5	−1.99	0.09
FR2	1285	1995	683	554	20	1.1	6.1	0	6.2	−2.03	0.01
F1	9192	1998	393	440	207	−26.8	16.7	7.4	11.5	−1.04	0.71
F1	7717	1998	277	591	56	−47.7	15	21.5	12.6	−1.04	0.77
F1	10909	1998	327	637	10	−38.4	13.9	22.8	13.4	−1.17	0.71
F2	4040	1998	348	747	433	−2.2	11.2	0.2	10.8	0.31	0.55
F2	5294	1998	326	978	202	−9.3	15.7	2.1	13.8	−0.37	0.78
F2	9193	1998	390	1124	56	−17.4	12.2	3.7	10.5	−1.46	0.53
F2	10907	1998	309	1170	10	−19.1[b]	11.9[b]	4.4[b]	11.5[b]	−1.67	0.4
F3	7066	1998	395	1224	413	−1.8	6.9	−0.1	9.2	0.35	0.1
F3	9403	1998	395	1581	56	−15.9	11.6	1.9	11	−1.09	0.68
F4	9708	1998	332	1777	207	−2.1	5.7	−1	7.2	0.07	0.04
F4	9194	1998	390	1928	56	−2.6	5.6	−0.5	7.1	−0.14	0.24
F4	9195	1998	376	1974	10	−6.3	7.2	1.8	7.4	−0.54	0.51

[a]The columns show: mooring name, instrument number, deployment year, length of record, instrument depth, instrument height above the bottom, mean velocity components (u positive eastward, v positive northward) and mean potential temperature with standard deviations.
[b]Compass malfunction. See discussion in text.

surface freezing point (∼−1.9°C), showing that these instruments are most of the time immersed in ISW. At S2 a total of 7 vectors are shown, obtained from deployments in 1977, 1985 and 1987. The flow has a mean northward component at positions S2 and S3 slightly north of the sill, and at FR1 south of the sill. At FR2 and at "S3", however, the flow is deflected slightly southward as a result of local topography.

Table 3. MicroCAT Summary Data[a]

Moor. Name	Instr. Number	Record Days	Obs Depth	mab, m	θ, °C	ϕ_θ, °C	S, psu	ϕ_S, psu
F1	137	393	638	9	−1.17	0.71	34.589	0.038
F2	138	391	1171	9	−1.63	0.39	34.592	0.024
F3	139	396	1628	9	−1.52	0.50	34.607	0.024
F4	140	390	1975	9	−0.57	0.52	34.642	0.027

[a]The columns show mooring name, instrument number, length of record, instrument depth, instrument height above the bottom, mean potential temperature and mean salinity with standard deviations.

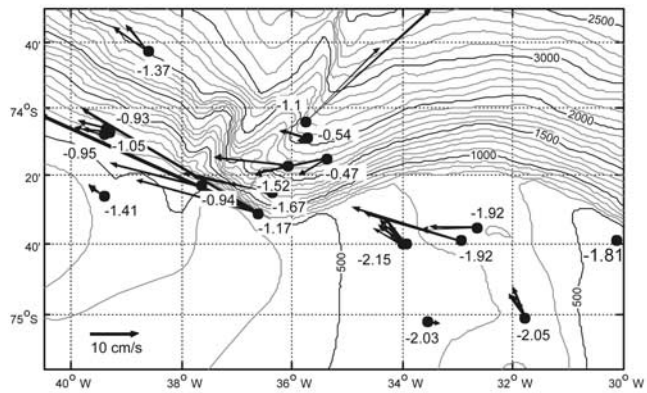

Figure 2. The mean current vector for each instrument. The numbers show the mean potential temperature (°C) of the deepest current-meter on each mooring. See also Table 2.

The mean northward speed component of the ISW at S2 was about 6 cm s^{-1} during 1985 (see Table 2).

[16] Further west, at the "F-section" across the slope, we note high velocities at F1 with an average speed >50 cm s^{-1} at 56 mab. The average speeds at 56 mab at F2 and F3 are also high, 19 cm s^{-1} and 16 cm s^{-1} respectively, while at F4 the average speed is 6.3 cm s^{-1}. At F1 there is a bottom layer more than 200 m thick with an average potential temperature <−1°C (see Table 2). The lowest average bottom potential temperature on the section, <−1.6°C, is found at F2. At 56 mab at F3 the average potential temperature is below −1.5°C, while the bottom layer at F4 is warmer, −0.5°C. Mooring F, positioned 34 km along the slope to the west of F1 and in water almost 180 m shallower (Figure 2), recorded an average speed of 20 cm s^{-1}, which is smaller than but comparable to that recorded by the upper F-section moorings. Even further west, at upper-slope moorings B1–B3 and C, the current speeds are much lower (∼6 cm s^{-1}).

[17] Further down-slope, at station D1 (2100 m depth), we again find high average velocities, ∼36 cm s^{-1}. Here the flow is northeastward, presumably diverted along isobaths by the ridge west of the D1 mooring. Even this far down the slope D1 instruments recorded an average potential temperature <−1°C. Mooring A, at ∼39°W near the 1900 m isobath ∼100 km west of D1, recorded an average current speed of ∼9 cm s^{-1} and a markedly lower average potential temperature (−1.37°C).

3.2. Temperature Variability

[18] Frequency distributions of potential temperature are highly informative about the water masses and mixing processes on the slope. Below we give a detailed description of these plots (shown in Figure 3), focusing on the instruments closest to the bottom.

3.2.1. Filchner Depression and Sill

[19] The FR1 and FR2 moorings south of the Filchner Depression sill, and the S2 and S3 moorings at the sill recorded ISW most of the time and only small temperature variance. The histograms for FR1 and S2 are shown in Figure 3.

3.2.2. Continental Slope, F1–F4

[20] At mooring F1, located on the shelf break ∼80 km west of S2 and only about 100 m deeper, the situation is quite different (Figure 3). The variance in temperature is large, with a sharp lower cut-off (−2.0°C) set by the potential temperature of the coldest ISW flowing over the sill, and a maximum potential temperature determined by the ambient WDW/MWDW at the depth of the instrument (0.5°C at 10 mab).

[21] At mooring F2 the average bottom potential temperature (−1.6°C) was distinctly lower than at F1, and water close to the freezing point was sometimes seen even at 433 mab (not shown). There is a sharp lower cut-off with a marked frequency peak at 10 mab but no upper cut-off, indicating less interaction of the cold plumes with the overlying WDW than at F1. The temperature variability at the F3 mooring is similar to F2, whereas the F4 mooring is dominated by the WDW and shows only a weak contribution from the plume waters.

3.2.3. Deep Moorings

[22] Potentially super-cooled waters were occasionally observed at D1 (2100 m depth) and D2 (1800 m depth) on the continental slope, showing that plumes of ISW can sometimes reach these depths almost without mixing (Figure 3). The peak in the distribution of T near 0°C at D2 suggests the frequent presence of unmodified WDW: this peak is missing at D1, further downstream and 300 m deeper than D2. We tentatively interpret this observation as indicating substantial mixing of the plume water and ambient water between these two locations.

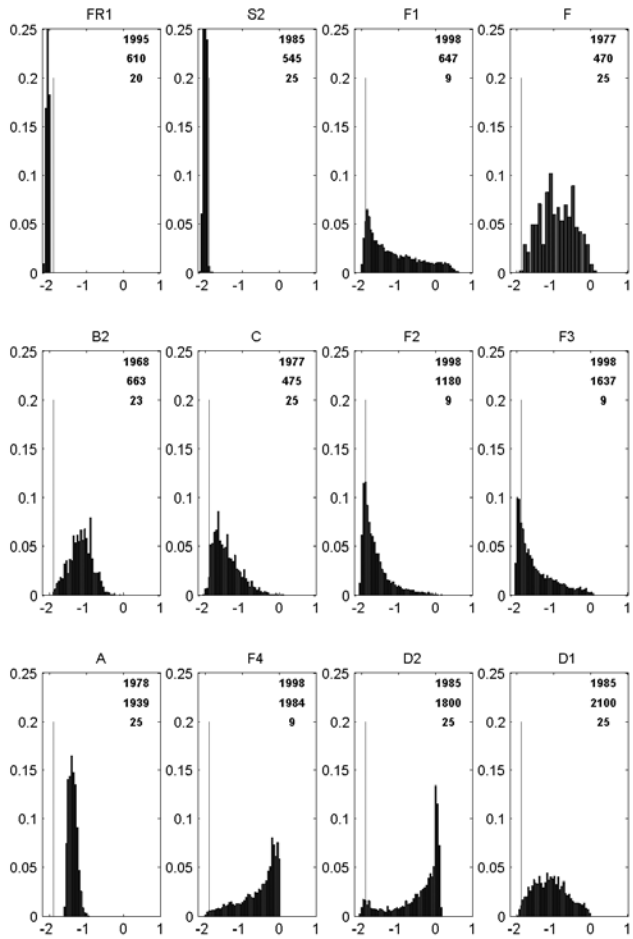

Figure 3. Histograms of the frequency of potential temperature from the deepest current meter at selected moorings. The temperature interval is 0.05°C except at *F* where it is 0.1°C. The numbers within the frames refer to year of deployment, depth of instrument and height above the bottom. The thin vertical line in each panel indicates −1.9°C. (Note at FR1 and S2 the maximum frequency exceeds 0.25).

[23] Data from mooring A at 1915 m depth and about 100 km further west (Figure 2), show, in dramatic contrast to the other deep moorings (D1, D2, F3 and F4) that the cold plume does not reach this location (Figure 3), at least in this year. The water at mooring A is well mixed with an average potential temperature −1.37°C at 25 mab and only slightly higher (−1.25°C) at 100 mab, see Table 2. There is no sign of ISW or WDW at this location.

3.2.4. Continental Shelf West of 38°W

[24] The B1, B2, B3 moorings are located a few miles apart on the upper slope at 600–660 m depth. The mean

potential temperatures here are around −1°C and the plot from the instrument at B2 in Figure 3 shows that the potential temperature rarely drops below −1.9°C. The potential temperature distribution at B2 (and at B1 and B3, not shown) shows little resemblance to the distribution at the F1 mooring, further east and at nearly the same (647 m) depth. The bell-shaped distribution looks more like that at mooring A, indicating that highly efficient mixing processes have taken place, see discussion section 6. The short duration F-mooring (32 days) located between F1and B1−B3 (see Figure 2) shows the same potential temperature distribution as the B-moorings.

[25] The C-mooring is located at 475 m depth on the shelf south of the B-moorings. The mean speed (4 cm s^{-1}) is lower than at B1−B3 and the mean potential temperature is markedly lower (∼−1.4°C). The C-record is distinctly different from the B1−B3 records, see Figure 3. The temperature record shows a lower cut-off set by the temperature of HSSW/WW, with a small fraction of ISW.

3.3. MicroCAT θ-S Observations at F-Section

[26] The high precision temperature and salinity data from the MicroCATs are shown as scatter plots of θ-S in Figure 4. The MicroCATs are located at the F1−F4 moorings (9 mab), see Figure 2. Water mass definitions according to *Carmack and Foster* [1975], as modified by *Grosfeld et al.* [2001], are also shown. The signature of ISW is clearly present at F1, F2, and F3, and covers a rather broad salinity range. The ambient WDW potential temperature at the depth of the MicroCAT at F4 is ∼0.0°C (see also Figure 3) and mixing products of WDW and cold plume water dominate the record in Figure 4, although even here there are a few recorded samples of unmixed ISW. There appears to be a slight shift toward higher salinity values at the deeper mooring sites, see also Table 3.

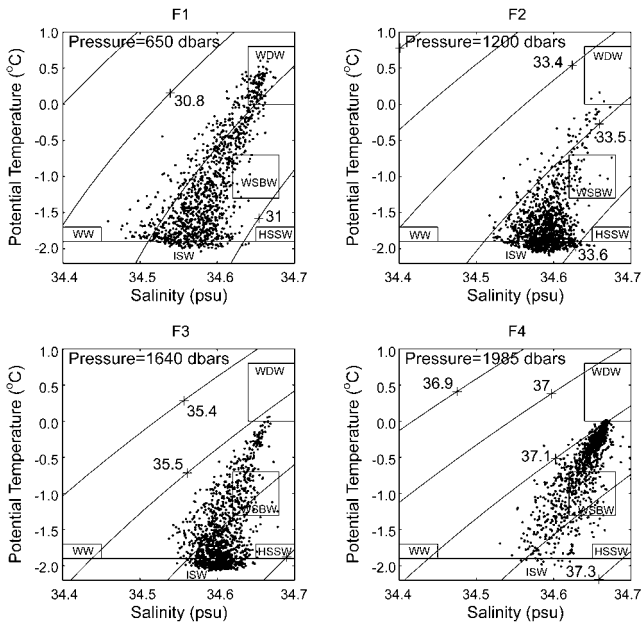

Figure 4. θ-S scatter plots from MicroCATs (observations every 4 hours) at the F-section at 9 mab. The in situ isopycnals (kg m^{-3}) are shown together with labels displaying water mass definitions.

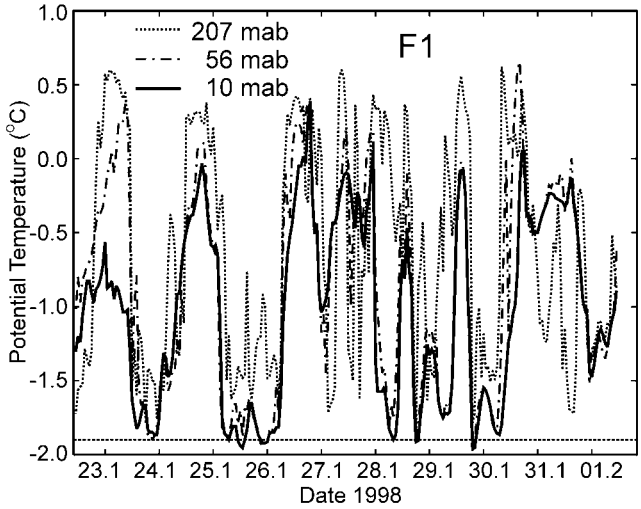

Figure 5. Ten days of potential temperature observations at 3 levels at mooring site F1. The dotted horizontal line shows the surface freezing point (−1.9°C).

[27] Figure 4 suggests the occurrence of diapycnal mixing between WDW and ISW-derived, low salinity water types near the freezing point. A 10-day sample of the potential temperature records from the F1-mooring instruments shows rapid alternations between cold and warm periods (Figure 5). Advection past the mooring of a rapidly changing water mass result in a T-S scatter plot implying more mixing than actually occurs.

[28] We do not observe Winter Water (WW) or High Salinity Shelf Water (HSSW) in any of the MicroCAT records from 9 mab on the F1−F4 moorings.

[29] The in situ isopycnal lines are shown in the θ-S plot in Figure 4. It appears that most of the ISW, and the products of mixing between ISW and WDW, are denser than the WDW and thus subject to down-slope buoyancy forcing all the way down the slope to >2000 m depth.

3.4. Plume Geometry and Variability

[30] A CTD section obtained during the recovery of the F1−F4 moorings is shown in Figure 6 together with the −1°C isotherm representing a 1-year average from the instrument moorings. In the CTD section the centre of the plume was found between the F2 and F3 moorings with a minimum potential temperature of −1.4°C near the bottom. The −1°C isotherm observed in the CTD section is located a few meters above the bottom and shows significant deviations from the annual mean obtained from the moorings. In fact, the cold plume was almost absent when this CTD section was taken. This is consistent with the non-stationarity of the plume, see Figure 5. Figure 5 also shows that when the plume is present at mooring F1 (bottom potential temperature <−1°C) it generally appears in a thick (>200 m) cold layer covering all instruments.

3.5. Interannual Variability

[31] The current meter observations are usually 1-year records, but some stations have been operated continuously for longer periods (see Table 2). Some stations have been repeated, e.g., 3 years at station S2. The average northward

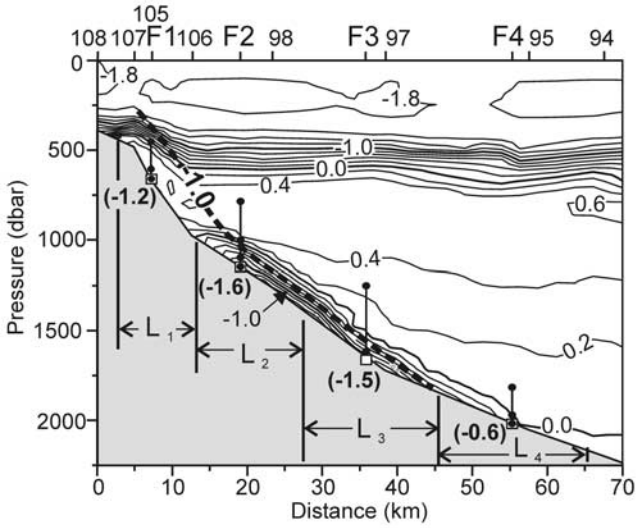

Figure 6. Potential temperature distribution at the F-section obtained during the recovery of the moorings (ANT XVI/2). The positions of the current meters (circles) and the MicroCATs (squares) are indicated. The one-year average of the $-1°C$ isotherm obtained from the current-meters is shown by the thick, dashed curve. The average potential temperatures (°C) from the MicroCATs are indicated in parentheses. The horizontal distances L_i used for transport calculations are indicated. Tick-marks on the top axis mark the location of the CTD casts.

component at the lower two current meters at the S2 site in 1977, 1985 and 1987 was 4.9 cm s^{-1}, 5.1 cm s^{-1} and 3.9 cm s^{-1}, respectively. The difference of 1 cm s^{-1} between these records are within the standard error, $\sim\pm1.3$ cm s^{-1}, see Table 2 and section 2. We are therefore unable to detect interannual variability in the current on the basis of the S2 data series. The three years of measurements at the S2 site may not, however, be strictly comparable. The 1987 position was located $\sim$2 km west of the 1977 and 1985 position, see Table 1. Because of the strong topographical steering on the sill even small differences in position may cause differences in the current, masking true interannual variations.

[32] The B1, B2 moorings from 1968 were discussed by *Foldvik et al.* [1985b] who noted the total breakdown at both moorings of the generally dominant diurnal tidal constituents in July 1968. The moorings were replaced by B3 in 1977. The record from B3 showed no collapse of the diurnal tide. On the basis of the temperature records, *Foldvik et al.* [1985b] speculated that the shelf waters in 1968 were almost homogenized and thus not able to sustain the baroclinic diurnal tide; see also the discussion by *Middelton et al.* [1987]. There was no significant difference in the average water speed at the B-moorings between 1968 and 1977.

[33] In Figure 7 we have presented one of the longest records available: the series from FR1, south of the Filchner Sill. This record demonstrates that northward flowing ISW occupies the deepest layer (below 232 mab) at all times. The upper instrument (353 mab) shows the influence of intruding MWDW in winter with a corresponding minimum in the northward velocity component. The seasonal differences in

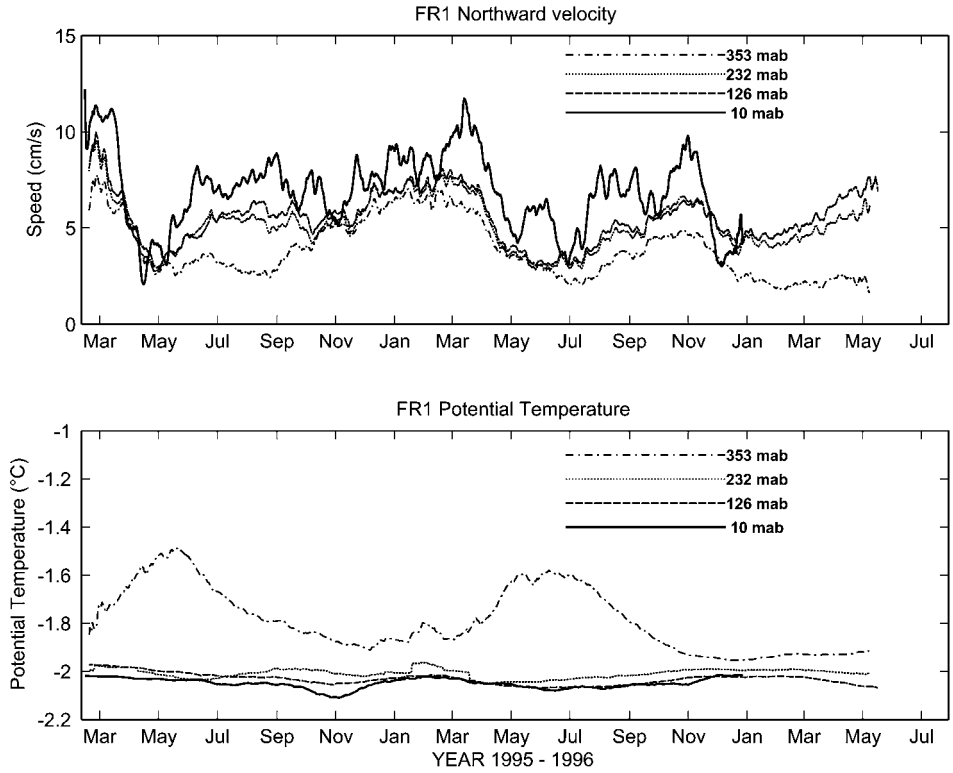

Figure 7. Time series of filtered (721 hour running average) meridional velocity component (upper panel) and potential temperature (lower panel) at mooring FR1 south of the Filchner Sill.

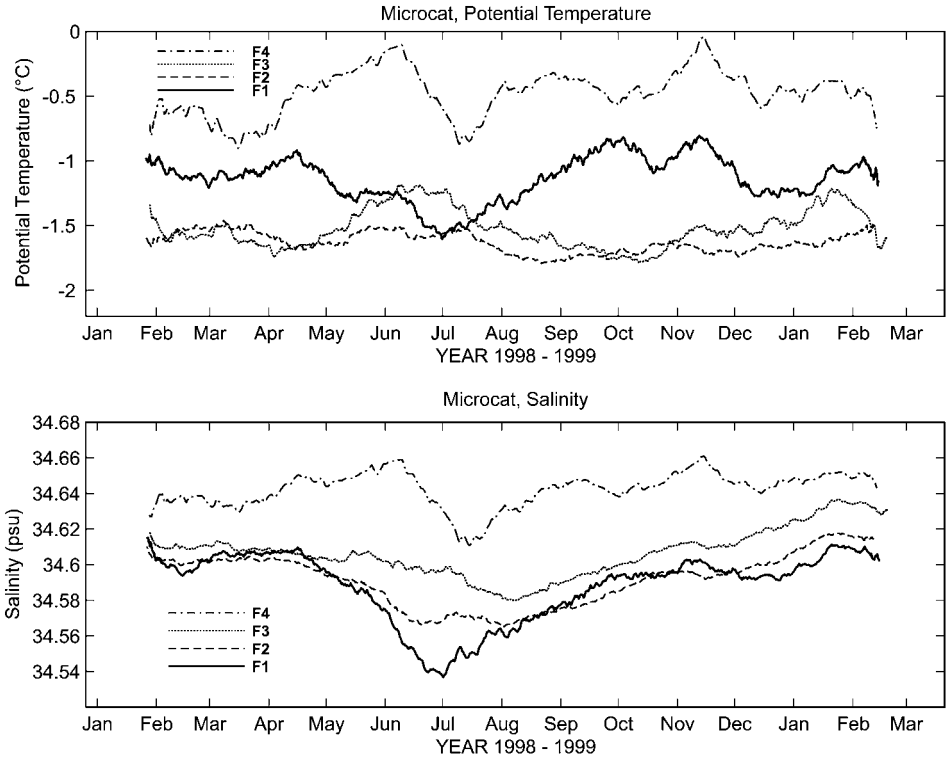

Figure 8. Time series of filtered (721 hour running average) potential temperature and salinity from MicroCAT instruments on section F.

the temperature of the ISW are <0.1°C, but the speed varies considerably, with a minimum in winter. The average speed at the lower current meter was 6.8 cm s^{-1} in 1995 and 7.2 cm s^{-1} in 1996. Again, the difference between the years is within our estimate of the standard error in the series.

[34] In Figure 8 we also show the potential temperature and salinity records for the MicroCATs on slope moorings F1–F4 and note the distinct salinity minimum at all moorings in winter. We do not see a similarly clear seasonal signal in the temperature except at F1, which shows a temperature minimum in winter. A direct consequence of the seasonal signal in the salinity of the overflow water is that a corresponding variability would be imprinted on any WSBW formed by mixing between plume water and the overlying MWDW/WDW. With typical deep water velocities of 1 cm s^{-1} the seasonal variability in salinity would be spread over 300 km.

4. Transport of Filchner Overflow Waters

[35] Our main motivation for this study was to calculate the rate of formation of WSBW that results from the overflow of cold, dense water from the Filchner region. We use the data sets from the F-section (F1–F4) and the S-section (S2, S3) to determine the volume flux from the shelf.

4.1. Method

[36] In order to compare the transport estimates from different sections all current meter measurements must be referred to a common temperature. The water mass in the S-section is almost undiluted ISW, whereas the F-section shows considerable mixing with MWDW or WDW. We shall assume that all plume water on the slope is formed by the mixing of cold shelf water originally at potential temperature θ_I with warmer water (WDW or MWDW) of potential temperature θ_w. A water parcel of temperature θ_i then consists of R_i parts of cold water and $(1 - R_i)$ parts of WDW, where

$$R_i = \frac{\theta_w - \theta_i}{\theta_w - \theta_I}$$

The flux of dense, cold water converted to potential temperature θ_I is then $v_{n,i}R_i$ where $v_{n,i}$ denotes the observed velocity component normal to the section. Thus the time-averaged flux of this cold water measured by a current meter (per unit area) becomes

$$f_n = \frac{1}{N}\sum v_{n,i} \cdot R_i \qquad (1)$$

where N denotes the number of observations. The values of θ_w for the F-section have been obtained from the potential temperature plots in Figure 3 (the high temperature cut-off) and CTD sections. Table 4 lists the values for θ_w and f_n. The calculated fluxes are relatively insensitive to θ_w: a variation in θ_w of 0.1°C changes the calculated transport by <2%. For the S-section we have derived θ_w from CTD sections only. High variability on the shelf makes the determination of θ_w difficult and somewhat arbitrarily we have put $\theta_w = 0.0$°C. However, at the S section the temperatures are close to θ_I and the choice of θ_w is not important. The results are more

Table 4. Transport of Cold Shelf Water Through the S-Section (1985) and the F-Section (1998)[a]

Mooring Name	Instr. Number	Obs Dep., m	mab, m	θ_w, °C	D, m	Fn, cm/s	L, km	Transport, Sv
S2	3160	355	190	0.0	90	2.1		0.1
S2	4223	445	100	0.0	83	4.1		0.2
S2	7716	520	25	0.0	63	6	65	0.2
S3	3164	510	100	0.0	173	6.3		0.8
S3	4277	580	25	0.0	63	7.2	72	0.3
Transport S-section								1.7
F1	9192	440	207	0.7	150	14.5		0.2
F1	7717	591	56	0.6	98	28.9		0.3
F1	10909	637	10	0.6	33	26.5	11	0.1
F2	4040	747	433	0.6	230	0.5		0.0
F2	5294	978	207	0.5	188	4.0		0.1
F2	9193	1124	56	0.5	98	13.2		0.2
F2	10907	1170	10	0.5	33	16.0	14	0.1
F3	7066	1224	413	0.4	358	0.1		0.0
F3	9403	1581	56	0.3	208	10.1		0.4
F3SC	139	1630	9	0.2	33	13.0	18	0.1
F4	9708	1777	207	0.2	150	0.2		0.0
F4	9194	1928	56	0.1	98	0.2		0.0
F4	9195	1974	10	0.1	33	2.0	20	0.0
Transport F-section								1.5

[a]The columns show: mooring name, instrument number, depth of instrument, distance of instrument above bottom, θ_w is the environmental potential temperature used for transport calculations, D denotes the thickness of the water column assigned to each instrument, F_n is the flux vector according to equation (1), L is the distance assigned to each mooring and the transport is given in Sverdrup (10^6 m^3 s^{-1}).

sensitive, however, to the reference temperature selected for the cold water. We use a value for θ_I of -1.9°C, the freezing point of seawater at surface pressure. If this reference temperature had instead been set at -2°C then the flux of cold shelf water would be reduced by approximately 10%. The calculated rate of bottom water production is unaffected by the value of θ_I.

[37] The flux of cold $\theta = \theta_I$ water recorded at a current meter mooring (per unit width) then becomes

$$F_n = \int f_n dz \tag{2}$$

[38] The vertical integration was carried out using an objective but necessarily arbitrary approach in which each instrument is taken to represent the section of water column from halfway to the instrument below to halfway to the instrument above. For the deepest instrument the integration starts at the bottom, whereas the upper instrument is assumed to represent a water column equal to the distance between the two upper instruments. Note that we have assumed that all plumes are derived from cold shelf water of potential temperature -1.9°C. All plumes with potential temperature below the ambient temperature θ_w contribute to the flux of the cold shelf water. This model does not discriminate between ISW and HSSW.

[39] Finally, the transport of cold shelf water, F, is obtained from the flux vectors $F_{n,j}$(2), thus

$$F = \sum L_j F_{n,j} \tag{3}$$

The summation in (3) goes over the number of current meter moorings and L_j denotes the length of the section to be represented by that mooring. The values of L_j are determined by the midpoints between moorings (Figure 6). The choice of the L_j at the flanks is discussed below. The error bars on the transport calculations are related to the geometry of the plume and are additional to the standard errors of the time series of water velocity (see section 2).

4.2. Transport Estimate for the S-Section

[40] We estimate the northward transport of cold water at the sill of the Filchner Depression using the S-section data for 1985, when records from the S2 and the S3 moorings were available simultaneously. Data from the S2-mooring are also available for 1977 and 1987; see our remarks in section 3.5 on interannual variability.

[41] Figure 9 shows the extent of ISW, defined by the -1.9°C isotherm, from CTD measurements made along the S-section during several Antarctic summer cruises. These snapshots suggest that the border of cold water is located between the 400- and 500-m isobaths on the west side of the Filchner Depression and between the 500- and 600-m isobaths on the east side. We use these observations to determine the L_1 and L_2 parameters for the S-section (see Figure 9 and Table 4). Figure 9 gives the impression of a sloshing motion of the ISW in the Depression, that is, there

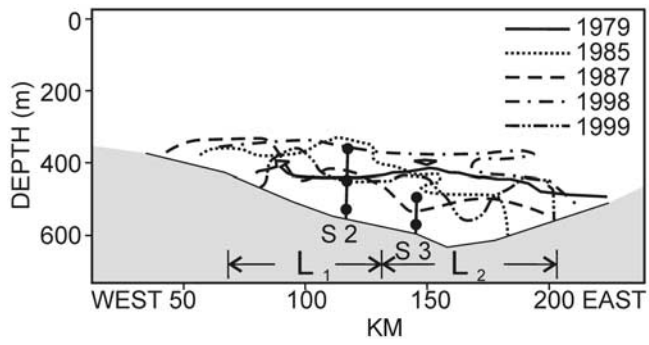

Figure 9. Position of the -1.9°C isotherms at the Filchner Sill along the S-section obtained from different summer expeditions. The current meter positions are indicated, and L_1, L_2 show the lengths used for transport calculations.

is a tendency for the cold water to be located higher on the western side when it is lower on the eastern side, and vice versa. This implies a certain reduction of the combined error bounds on $L_1 + L_2$, although this is not taken into account in the error estimates below.

[42] The data from the upper instrument (190 mab) on the S2 mooring show that about 15% of the measurements are below −1.9°C whereas at the instrument below (100 mab) 85% of the measurements are below −1.9°C. For the purposes of this calculation, therefore, we assume that the average position of the −1.9°C isotherm is around 145 mab. This position is in reasonable agreement with the CTD observations in Figure 9.

[43] The two current meters at S3 are not sufficient to resolve the thickness of the cold-water layer at that site. From Figure 9, however, it seems reasonable to assume the average thickness of ISW to be the same as at S2. To reflect this argument the upper instrument at S3 has been taken to represent a correspondingly thicker water column (see Table 4). Since the upper instrument at S2 shows smaller velocities than below it, this procedure might lead to a slight overestimate of the transport at S3.

[44] Using the above methodology, we estimate that the transport across the S-section (Table 4) during 1985 was 1.7 ± 0.5 Sv. The error estimate is related to the L_j values on the flanks, the thickness allocated to the upper instrument and the standard error of the mean current.

4.3. Transport Estimate for the F-Section

[45] The in situ isopycnal lines (referenced to 650 m) at F1 are shown in the θ-S plot in Figure 4a. It appears that ISW and its mixing products are usually denser than WDW and thus capable of sinking further down the continental slope. However, some of the cold, low salinity water at mooring F1 appears to be slightly lighter than the core of WDW. In order not to overestimate the contribution of cold shelf water at F1 we eliminate from the transport estimate all water appearing lighter than the core value of the WDW, ~30.89 kg m^{-3}. Thus all observations having in situ densities less than 30.89 kg m^{-3} are excluded from the integration (2). This excludes 17% of the observations. The sensitivity of the choice for the limiting isopycnal was tested by bracketing the selection: choosing 30.88 kg m^{-3} and 30.90 kg m^{-3} results in excluding 7% and 24% of observations, respectively.

[46] As seen from Figure 2 and Table 2, the velocities are very high at the F1 mooring. This implies that our calculation of cold-water flux using equation (3) is quite sensitive to the determination of the assigned cross-slope length L_1. As mentioned above, the border of cold shelf water at the S-section was located between the 400- and 500-m isobaths. Since the flow on the shelf is so strongly controlled by topography, and since the distance between the shallow side of these two sections is rather short, we shall assume that the same borders apply to the S- and F-sections: i.e., since the out-flowing cold water resides over the 400-m isobath at the S-section, we assume that the edge of the cold water plume is near the 400-m isobath at the F- section. The consequent choices of L-values are shown in Figure 6.

[47] With these choices (3) implies that the flux of −1.9°C water leaving the shelf through the F-section in 1998 was 1.5 ± 0.3 Sv (see Table 4). In addition to the standard error of the mean current (section 2) the largest components in the estimated error are the value of L1 and the choice of isopycnal determining the data points that contribute to the estimate of the F1 flux. Within the error bounds, the transport of ISW over the Filchner sill is the same as through the F-section, however flow rates are much higher in the latter section. The weak stratification suggests that most of the flow will follow lines of constant f/H: the acceleration arises because the isobaths converge dramatically between the sill and the F-section.

5. Production of WSBW

[48] Having computed the flux of cold (<−1.9°C) water leaving the shelf we may now estimate the rate of change of mass flux based on the observed hydrography. We assume that WDW is entrained into the cold plume and that no plume water is detrained into the overlying WDW. This assumption is supported by CTD measurements from the area over several field seasons (see, for example, the 1990 measurements shown in Figure 10). The general impression from CTD measurements, from the yearlong MicroCAT records shown in Figure 4 and from the potential temperature records from D1 (Figure 3) is that the cold shelf water sometimes reaches depths greater than 2000 m with little mixing with the overlying water.

[49] We denote the plume properties with the index p, the properties of the WDW with the index w and entrainment with the index e. As a result of entrainment of m_e of the overlying WDW, a parcel of plume water m_p increases its mass by dm_p and its temperature by $d\theta_p$. Continuity of heat and mass is then expressed by

$$m_p\theta_p + m_e\theta_w = (\theta_p + d\theta_p)(m_p + dm_p) \tag{4}$$

where

$$m_e = dm_p$$

thus

$$(\theta_w - \theta_p - d\theta_p)dm_p = m_p d\theta_p \tag{5}$$

In (5) the second order term will be neglected. The equation may then be integrated to obtain

$$m_{p,1} = m_{p,0} e^{\int_0^1 \frac{d\theta_p}{\theta_w - \theta_p}}. \tag{6}$$

(A similar equation applies based on the continuity of salt).

[50] Here index 0 and 1 refer to the initial and to the end state, respectively. The integral in (6) may easily be calculated by stepwise integration since the temperatures of the WDW and the plume are known (see Figure 10). Since the temperature of the WDW decreases with depth it follows that the production of deep-water is more efficient when the mixing takes place at large depths.

[51] Note that if θ_w is constant (6) takes the form

$$m_{p,1} = m_{p,0} \frac{(\theta_w - \theta_p)_0}{(\theta_w - \theta_p)_1}. \tag{7}$$

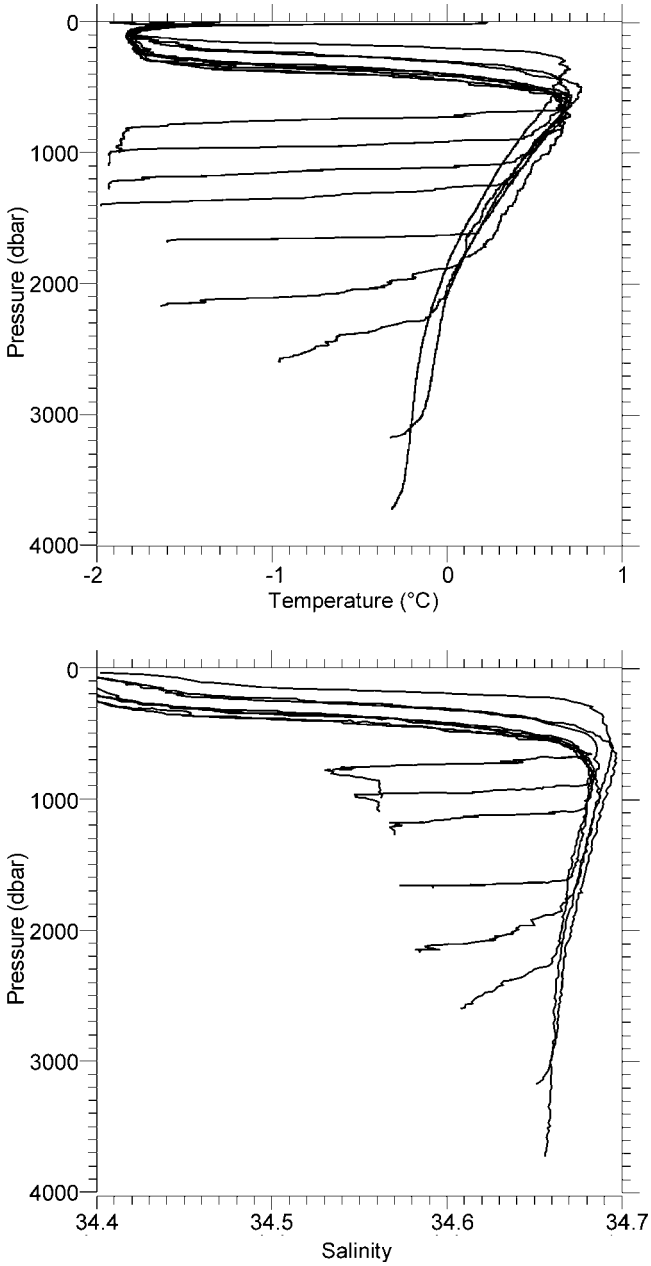

Figure 10. Ensemble of θ-S profiles at the slope obtained during the Norwegian Antarctic Expedition 1990. The location of the section is shown in Figure 1b.

If all mixing did take place at 2000 m depth then Figure 10 gives θ_w as 0.0°C, $\theta_{p,0} = -1.9$°C, and $\theta_{p,1} = -0.8$°C. Thus we obtain $m_{p,1} = 2.5\ m_{p,0}$, that is, the production of bottom water referenced to −0.8°C is 2.5 times the flux of cold water leaving the shelf. If the mixing took place at 3000 m depth, however, where $\theta_w = -0.2$°C, we obtain $m_{p,1} = 3m_{p,0}$. Stepwise integration of (6) using values of θ_w from Figure 10 gives $m_{p,1} = 2.7m_{p,0}$. This compares well with model experiments by *Killworth* [1977] and *Alendal et al.* [1994] who found that the volume flux at 2000 m depth should increase by 2 to 3 times the initial value. In the following we apply the factor 2.7 to estimate the production of WSBW. In a recent theoretical study *Holland et al.* [2002] find that the volume flux should increase by a factor close to two due to mixing in a single strong hydraulic jump. When the effects of increased buoyancy due to thermobaricity, boundary layer mixing, and shear instability are considered, the factor 2.7 adopted above seem reasonable.

6. Discussion

[52] The broad picture that emerges from the data presented here is that large volumes of cold shelf water flow northward over the sill in the Filchner Depression and toward the continental shelf break. At moorings S2 and S3, located on Filchner Sill, the deepest instruments indicate pure ISW with very small temperature variance. The flow accelerates as it descends the upper slope, turns to the left (westward) under the influence of the Coriolis force and accelerates further as the continental slope from 400–700 m depth steepens (isobaths converge) between the Filchner Depression and the F-section. The further fate of the flow depends on both internal plume dynamics and the local forcing, such as the phase of time dependent phenomena like tides, shelf waves, the position of the Antarctic Slope Front, and weather forcing. Below we consider some factors that determine the pathways of cold shelf waters entering the deep Weddell Sea circulation.

6.1. Short-Term Variability

[53] The B1, B2 and B3 records were discussed by *Foldvik et al.* [1985b] who noted the exceptionally strong diurnal tidal currents near the shelf break. Tides in the area are also discussed by *Middelton et al.* [1987], *Foldvik et al.* [1990], *Robertson et al.* [1998] and *Padman and Kottmeier* [2000]. In addition to the strong tidal regime we observe marked wave disturbances at lower frequency on the slope. Figures 11a and 11b show 10- and 12-day segments of the de-tided current meter records from the F1 and F4 moorings, respectively. At F1 the average current dominates and has wave disturbances superimposed. At F4 the mean current is weaker and the flow is dominated by strong shelf waves with periods of ∼3–6 days. Such waves may cause cross-slope advection and thus be important for the fate of the cold plumes. The structure of low-frequency (weather band) shelf waves on the southern Weddell Sea continental

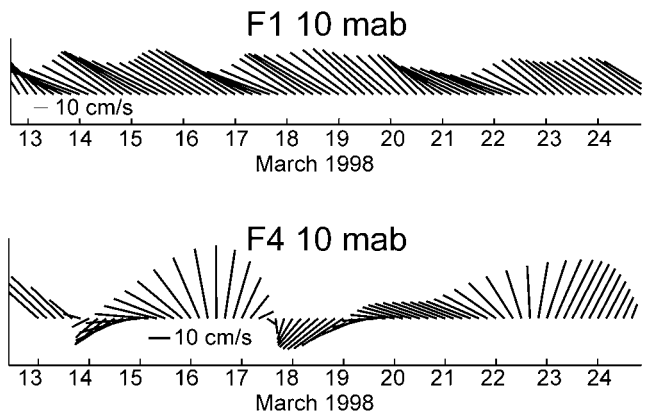

Figure 11. Twelve days of the de-tided current vectors 10 mab, displayed at 4-hour intervals, at F1 (upper panel) and F4 (lower panel).

slope was discussed by *Middelton et al.* [1982], while *Foster et al.* [1987] discussed the potential role of these waves on water mass transformation along the shelf break.

6.2. Comments on Plume Dynamics

[54] The frequency of ISW at the F1, F2, F3 and F4 moorings, defined by the relative number of observations of potential temperature below the surface freezing point, is 8%, 27%, 28% and 1%, respectively. These observations are consistent with ISW flowing over the sill and being turned westward by the Coriolis force. They also show that the coldest plumes rapidly advance down, as well as along the slope.

[55] There are two main dynamical reasons why the cold plumes occasionally may reach the deepest current meter sites (F4 and D1) without significant water mass modification. First, the decrease in buoyancy as a result of mixing is counteracted by the thermobaric effect [*Killworth*, 1977], that is, the increase in density with increasing pressure is larger in the cold plumes than in the adjacent WDW. This effect is clearly revealed by comparing the MicroCAT plots in Figure 4, where the density contrast between the WDW and the bulk of the ISW is seen to increase with depth. Second, from density profiles calculated from CTD measurements we may estimate the phase speed, $c = \sqrt{(g'H)}$, for long waves at the ISW-WDW interface. Here H denotes the thickness of the plume, $g' = g\Delta\rho/\rho$ is the reduced gravity and $\Delta\rho/\rho$ denotes the interfacial relative density anomaly. We find maximum phase speeds of about 0.4 m s^{-1}, obtained for a plume thickness 200 m (indicated by the cold water events in Figure 5) and interfacial relative density anomaly of 1.0×10^{-4} kg m^{-3} (as defined by the typical difference between observed density and the WDW density in Figure 4). In Figure 12 we show the joint distribution of θ and |U| near the sea-bed at 4 moorings, F1, F2, D2 and D1. Depending on the actual thickness of the plume, the distribution of |U| suggests that at each site, the flow is supercritical (that is, the plume speed is larger than the internal phase speed) for some fraction of each total record. For supercritical flows, resonance waves (lee waves) do not form. Thus the associated mesoscale mixing behind irregularities in the bottom topography is strongly reduced [*Long*, 1954]. These dense plumes may therefore reach great depths with little mixing and much reduced friction. The strong correlation between high speed and low temperature at D1 and D2 (Figure 12) supports our view of the efficiency of this mechanism.

6.3. Supercritical Flows and Mixing

[56] On the continental slope the overflowing shelf waters may attain supercritical speed as a result of flow convergence and/or down-slope buoyancy forcing aided by thermobaricity. Flow convergence accelerates the entire water column and does not discriminate between water types, whereas down-slope buoyancy forcing aided by thermobaricity acts only on the cold plumes. This is clearly demonstrated in the potential temperature-speed plots in Figure 12 where a strong correlation is clearly visible between high speed and low temperatures at moorings D1 and D2, but not at moorings F1 and F2. The transition to sub-critical speed takes place when the slope becomes less steep and may be

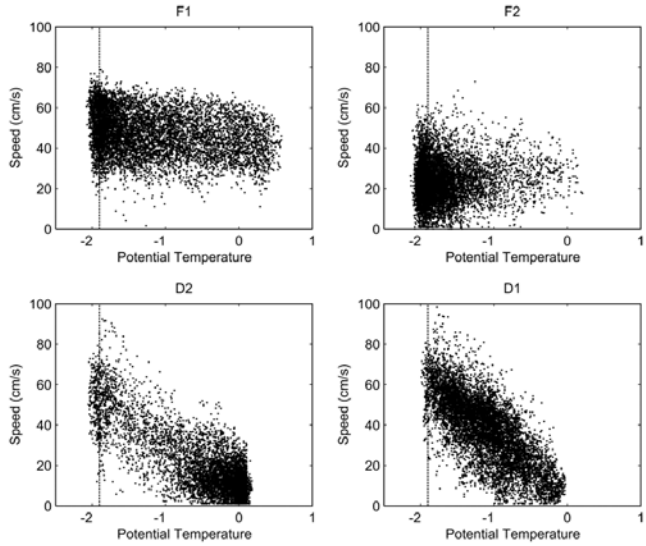

Figure 12. Scatter plots of potential potential temperature versus speed for selected current-meter records close to the bottom. See Figure 1b and Table 2 for locations and details.

accompanied by violent mixing associated with a hydraulic jump, [*Long*, 1954; *Holland et al.*, 2002].

[57] The average speed at F1 is very high (45 cm s^{-1}) and much of the flow at F1 is believed to be supercritical. At mooring *F* the speed is reduced but still high (20 cm s^{-1}) whereas at the B-moorings the speed is low (6 cm s^{-1}). These differences seem to be governed by isobath divergence (Figure 2). The temperature distribution at F1 is quite different from that at the S-moorings (Figure 3). The variance is large, with a sharp lower cut-off at −2.0°C determined by the parent ISW, and a potential temperature maximum (0.5°C at 10 mab) determined by the temperature of the overlying WDW/MWDW. The temperature distributions at the F-mooring (only 32 days long) and the B-moorings are entirely different to that from F1. The lower cut-off is absent, the frequency distribution is nearly bell-shaped and the mean temperature is close to −1.0°C. Since much of the flow changes from supercritical to sub-critical between F1 and the *F* we believe that this shift in temperature distribution accomplished over such a very short distance (∼20 nm) is mostly due to mixing by hydraulic jumps. Such mixing of plume water with overlying WDW will systematically increase the temperature of the water samples, as observed. Cross-slope advection may also affect the temperature distributions, but cross-slope advection of (sharp) frontal gradients tends to produce a two-peak distribution with upper and lower cut-offs.

[58] The C- mooring on the nearby shelf (Figure 2) yielded a temperature distribution (Figure 3) with a sharp lower cut-off and a mean potential temperature close to −1.5°C. This is shelf water, WW or HSSW with a minor contribution of ISW, and does not reveal the same mixing history as that at the neighboring F- and the B-moorings.

[59] Much of the overflow descends as bottom-trapped cold plumes east of ∼37°W. The highest fraction of ISW

is found in the F-section at moorings F2 and F3, that is, between the ~1200- and ~1600-m isobaths (see Figure 6), with an average potential temperature of −1.67°C and −1.52°C, respectively. At the continental slope east of 38°W the variability of currents and temperature is high (Table 2 and Figures 3, 11 and 12). The temperature distributions at F2 and F3 show a sharp lower cut-off set by the temperature of the ISW at the sill, but no clear upper cut-off at the temperature of the WDW. This indicates that very little mixing has taken place between the plume and the overlying water during the journey from the sill to the F2- and F3-moorings. As discussed in section 6.2, a low level of mixing is consistent with the suppression of resonance wave-induced meso-scale mixing in the often-supercritical flow observed at F2 and F3 (Figure 12). West of the F-section the cold flow encounters rough topography, including two prominent ridges. On the basis of the map in Figure 2 we anticipate that most of the flow passing between F2 and F3 will be steered by the ridge between 38°W and 37°W. On the western side of that ridge the topography appears less steep and a transition from supercritical to sub-critical flow is likely, with consequent mixing in hydraulic jumps. Mooring A is located near the 2000-m isobath and ~100 km downstream from F2–F3. Temperatures recorded at this mooring are consistent with the above picture, indicating only the product of mixing between WDW and ISW, and not the parent water masses themselves (Figure 3). The cold plume therefore never reaches this location. At mooring A the water is well mixed with an average potential temperature of −1.37°C at 25 mab and only slightly higher (−1.25°C) at 125 mab. The temperature distribution at A is the signature of a new boundary layer water mass: Newly Formed WSBW, produced by mixing of cold shelf water plumes (ISW/HSSW) and warmer WDW. Since there is no sign of WDW at the upper instrument (125 mab) the average thickness of this boundary layer must be well above 125 m, say ~200 m thick. The width of the layer must be larger than the horizontal excursion from shelf waves, on the order of 70 km in the example in Figure 11b. At an average speed of ~9 cm s^{-1}, the above figures indicate a transport within this boundary layer of ~0.8 Sv when referenced to −1.9°C.

[60] The high north-eastward mean speed at mooring D1 (see Figure 2) is surprising, given its proximity to mooring F4 which has a much weaker mean flow. The ridge extending across the slope near 36°W (see Figure 2) must play a major role in steering this benthic flow. On the basis of local topography, CTD observations and observed velocities (Table 2) we have estimated the volume transport at D1 to be ~0.2 Sv. The bell-shaped temperature distribution at D1 is similar to that at *F* and B1-3 which we attributed to mixing during hydraulic jumps. However, a large portion of the observations at D1 show supercritical flow which may indicate the subsequent acceleration by flow convergence as the flow encountered the ridge at 36°W. The temperature distribution at mooring D2 shows clear upper and lower cut-offs set by the temperatures of WDW and ISW, respectively. The minimum separating the two peaks in Figure 3 suggests that little mixing has taken place. The average potential temperature at D2 (−0.47°C) is higher than at D1 (−1.10°C), indicating that the flow at D2 has a lower contribution from cold plumes. This suggests that the location of mooring D2 is near the deep limit for cold plumes on the slope.

6.4. Plume Pathways

[61] On the basis of the above interpretation of observations we have identified three pathways for the Filchner Overflow (FO) waters (Figure 1b):

[62] The FO1 path involves flow crossing the F-section near mooring F1 and being constrained to flow along the shelf break and upper slope. The FO1 plume is presumably located slightly down-slope of the F- and B1–B3 moorings and was detected by the dense network of five CTD sections covering the shelf and slope between 37°W and 40°W [*Foster et al.*, 1987]. These sections show cold water (~−1°C) centred on the slope, located between approximately 600 and 800 m depth. Presumably, the water in FO1 will continue westward in quasi-geostrophic balance with only a slow down-slope migration.

[63] The FO2 path is taken by cold plumes crossing the F-section in the area of F2 and F3 and arriving in the area of the mooring A as a well-mixed boundary layer water mass. FO2 appears in the CTD section reported by *Foster and Carmack* [1976] as a distinct, cold (<−0.8°C) layer located between 2000 m and 3500 m depth. FO2 also appears in all five CTD sections reported by *Foster et al.* [1987] as a cold, low salinity boundary current located around 2000 m depth. Like FO1, the well-mixed FO2 waters may continue westward in quasi-geostrophic balance, only slowly increasing in depth.

[64] The FO3 path is represented by the high speed current at mooring D1, directed toward the NE by the ridge close to 36°W (Figure 2). Since the flow at D1 is partly supercritical further strong mixing must be expected downstream as the slope becomes less steep.

[65] The width of the arrows in Figure 1b is not indicative of the relative strength of these currents, although the volume flux of FO3 is probably the smallest. The high variability on the slope implies variability in the location of these pathways (see also the CTD sections of *Foster et al.* [1987]). In addition to the pathways identified above (and possibly others that have escaped our sparse network of instruments) an Ekman mass flux is directed downslope in the benthic layer, aided by thermobaricity. This thin, cold, bottom layer is observed in almost every CTD cast in the overflow area in which the instrument is lowered close to the sea floor. *Tanaka and Akitomo* [2000] find that the Ekman transport in the Weddell Sea contributes ~1 Sv to the formation rate of WSBW.

[66] The above interpretation of currents suggests that the ultimate fate of cold shelf waters emanating from the Filchner Depression depends upon the depth that the plume reaches shortly after crossing the sill. This in turn depends on such factors as the location (depth) the plume crosses the sill, high-frequency variability due to tidal motion, shelf waves and instabilities in the Antarctic Slope Front. Processes such as these are able to advect fluid parcels across a wide range of depths, so that the flow of ISW may quickly be switched between a "shelf-break" path and a mid-slope path. Once advected to a critical depth on the slope thermobaricity takes hold and

Table 5. Estimate of WSBW Production Rates[a]

Authors	Method	Production Rate Sv	WSBW Temperature
Carmack and Foster [1975]	Deep sea current measurements, geostrophy and budget estimates.	2–5	−0.8°C[b]
Foster and Carmack [1976]	Heat and salt budget and shelf break mixing model	3.6	−1.3°C
Weiss et al. [1979]	Isotope data: $d^{18}O$ (Tritium)	5 (2.9)	<−0.9°C
Foldvik et al. [1985a]	Currentmeter moorings at Filchner sill and hydrography	2–5	−0.8°C
Gordon et al. [1993]	Ice Station Weddell, hydrography	3	<−0.8°C
Fahrbach et al. [1995]	Joinville - Kap Norvegia transect, currentmeter moorings and hydrography	2.2[c]	<−0.7°C
Muench and Gordon [1995]	Ice Station Weddell, current measurements and hydrography	2.5–3	−0.8°C
Weppernig et al. [1996]	Ice Station Weddell drift track. Isotope data.	5	−0.7°C
Mensch et al. [1997]	Tritium and CFC data. Southern and western Weddell Sea.	3.5	<−1°C
Mensch et al. [1998]	Tritium and CFC data from Ice Station Weddell drift track.	5[e]	−0.8°C
Gordon [1998]	Ice Station Weddell, hydrography and current measurements.	3–4	< −0.7°C[d]
Fahrbach et al. [2001]	Joinville - Kap Norvegia transect, multi year currentmeter moorings and hydrography	1.1–1.5	−0.7°C
Gordon et al. [2001]	Current profiler and hydrography. Ice Station Weddell and DOVETAIL data.	5	<−0.7°C
Naveira Garabato et al. [2002]	Current profiler and hydrography	4.5 ± 0.9	<−0.7°C
This study	Current measurements and hydrography	4.3 ± 1.4	<−0.8°C

[a]Updated from *Orsi et al.* [1999].
[b]Produced with shelf water temperature between −1.2°C and −1.4°C.
[c]Varying between 0.8 Sv and 3.9 Sv.
[d]Average temp. −1.1°C.
[e]Produced west of the drift track.

an ISW parcel is unable to return. The possibility that high-frequency processes determine the fate of ISW suggests that ISW "plumes" may be better considered as variable streams of ISW filaments or eddies. If this is the case, simple steady state models of plumes [e.g., *Killworth*, 1977] may not correctly represent the pathways and mixing of shelf-derived cold water.

6.5. Transport of Cold Shelf Water

[67] The calculated transport of cold shelf water crossing the S-section (Figure 9), 1.7 ± 0.5 Sv, is not significantly different from the 1.5 ± 0.3 Sv calculated for the F-section (Figure 6). The agreement between these estimates is remarkable considering they have been obtained for different sections and for different years. The implications of this agreement are firstly, that all the water leaving the sill (via the S-section) later passes through the F-section, none passing higher or lower on the slope, and second, that the transport has not changed significantly over the 13-years that separated the S- and F-section deployments. A large fraction of the overflow at the Filchner Sill originates as HSSW formed north of Ronne Ice Front (Figure 1) and flows around Berkner Island before arriving at the sill of the Filchner Depression [*Foldvik et al.*, 2001; *Nicholls et al.*, 2001]. Data from moorings installed beneath the ice shelf at the southern tip of Berkner Island indicate large interannual variability in the flow, which could lead to a similar signal in the overflow [*Nicholls and Østerhus*, 2003]. A major geophysical event occurred in the Filchner Depression in August 1986, between the two S2 deployments in 1985 and 1987. Giant icebergs broke away from Filchner Ice Shelf and subsequently grounded north of Berkner Island. Some change in the outflow would therefore be expected between 1985 and 1987 [*Nøst and Østerhus*, 1998; *Grosfeld et al.*, 2001]. However, as discussed in section 3.5 the estimated fluxes for 1985 and 1987 agree within the error bounds. We are not able to detect significant inter annual variations in the outflow.

[68] We conclude that the volume transport of the cold (−1.9°C) shelf water plume leaving the area of the Filchner Depression in the southern Weddell Sea is

$$F = 1.6 \pm 0.5 Sv. \quad (8)$$

6.6. Production of WSBW

[69] Production of WSBW by mixing cold and dense shelf waters (ISW) with overlying WDW was discussed in section 5. From (8), and using the conversion factor of 2.7 found in section 5, the production of newly formed WSBW, referenced to −0.8°C, becomes:

$$F_{WSBW} = 4.3 \pm 1.4 Sv. \quad (9)$$

[70] Table 5 lists estimates of WSBW production rates obtained by different authors using widely different approaches. Our estimate lies near the upper end of previously published assessments.

[71] Our estimate of the formation rate of WSBW is a lower bound on the rate of production from the region as a whole, as it does not account for sources other than the Filchner outflow (for example, shelves in the western Weddell Sea) [*Gordon et al.*, 1993]. We assume, however, that the FO1 plume identified at ∼40°W and at 600–800 m depth descends slowly along the western continental margin and therefore is likely to cross the section with long term moorings on the continental slope off the Antarctic Peninsula where a transport of WSBW of 1.3 ± 0.4 Sv was estimated by *Fahrbach et al.* [2001]. Also, the FO1 is likely to cross from west to east the track of Ice Station Weddell [*Muench and Gordon*, 1995], consistent with the observations and analysis of *Weppernig et al.* [1996]. Some of the 2–3 Sv of newly formed WSBW detected at the drifting station might therefore originate in the Filchner area.

[72] **Acknowledgments.** The authors wish to express their gratitude to the researchers and ship crews from all the expeditions to the region of the Filchner overflow that have contributed to this study. The oceanography

programmes on all Norwegian Antarctic Research Expeditions have been supported by the Norwegian Research Council who also supported participation in other expeditions. We gratefully acknowledge this long-term support. L.P. was funded by the National Science Foundation, grant OPP-9896006.

References

Alendal, G., H. Drange, and P. M. Haugan (1994), Modelling of Deep-Sea gravity currents using an integrated plume model, in *The Polar Oceans and their Role in Shaping the Global Environment*, *Geophys. Monogr. Ser.*, vol. 84, edited by O. M. Johannessen, R. D. Muench and J. E. Overland, pp. 237–246, AGU, Washington, D. C.

Carmack, E. C., and T. D. Foster (1975), Circulation and distribution of oceanographic properties near the Filchner Ice Shelf, *Deep Sea Res.*, *22*, 77–99.

Fahrbach, E., and S. el Naggar (2001), The Expeditions ANTARKTIS XVI/1–2 of the Research Vessel "POLARSTERN" in 1998/1999, *Ber. Polar- und Meeresforsch.*, *380*, 177 pp.

Fahrbach, E., G. Rohardt, N. Scheele, M. Schröder, V. Strass, and A. Wisotzki (1995), Formation and discharge of deep and bottom water in the northwestern Weddell Sea, *J. Mar. Res.*, *53*, 515–538.

Fahrbach, E., S. Harms, G. Rohardt, M. Schröder, and R. A. Woodgate (2001), Flow of bottom water in the Weddell Sea, *J. Geophys. Res.*, *106*, 761–778.

Foldvik, A., and T. Gammelsrød (1988), Notes on southern-ocean hydrography, sea-ice and bottom water formation, *Paleogeogr. Paleoclimatol. Paleoecol.*, *67*, 3–17.

Foldvik, A., T. Gammelsrød, and T. Tørresen (1985a), Circulation and water masses on the southern Weddell Sea shelf, in *Oceanology of the Antarctic Continental Shelf*, *Antarct. Res. Ser.*, vol. 43, edited by S. S. Jacobs, pp. 5–20, AGU, Washington, D. C.

Foldvik, A., T. Kvinge, and T. Tørresen (1985b), Bottom currents near the continental shelf break in the Weddell Sea, in *Oceanology of the Antarctic Continental Shelf*, *Antarct. Res. Ser.*, vol. 43, edited by S. S. Jacobs, pp. 21–34, AGU, Washington, D. C.

Foldvik, A., J. H. Middleton, and T. D. Foster (1990), The tides of the southern Weddell Sea, *Deep Sea Res.*, *37*, 1345–1362.

Foldvik, A., T. Gammelsrød, E. Nygaard, and S. Østerhus (2001), Current measurements near Ronne Ice Shelf: Implications for circulation and melting, *J. Geophys. Res.*, *106*, 4463–4477.

Foster, T. D., and E. C. Carmack (1976), Frontal zone mixing and Antarctic Bottom Water formation in the southern Weddell Sea, *Deep Sea Res.*, *23*, 301–317.

Foster, T. D., A. Foldvik, and J. H. Middleton (1987), Mixing and bottom water formation in the shelf break region of the southern Weddell Sea, *Deep Sea Res.*, *34*, 1771–1794.

Gammelsrød, T., A. Foldvik, O. A. Nøst, Ø. Skagseth, L. G. Anderson, E. Fogelqvist, K. Olsson, T. Tanhua, E. P. Jones, and S. Østerhus (1994), Distribution of water masses on the continental shelf in the southern Weddell Sea, in *The Polar Oceans and Their Role in Shaping the Global Environment*, *Geophys. Monogr. Ser.*, vol. 84, edited by O. M. Johannessen, R. D. Muench, and J. E. Overland, pp. 159–176, AGU, Washington, D. C.

Gordon, A. L. (1998), Western Weddell Sea thermohaline stratification, in *Ocean, Ice and Atmosphere: Interactions at the Antarctic Continental Margin*, *Antarct. Res. Ser.*, vol. 75, edited by S. S. Jacobs and R. F. Weiss, pp. 215–240, AGU, Washington, D. C.

Gordon, A. L., B. A. Huber, H. H. Hellmer, and A. Ffield (1993), Deep and bottom water of the Weddell Sea's western rim, *Science*, *262*, 95–97.

Gordon, A. L., M. Visbeck, and B. Huber (2001), Export of Weddell Sea deep and bottom water, *J. Geophys. Res.*, *106*, 9005–9017.

Grosfeld, K., M. Schröder, E. Fahrbach, R. Gerdes, and A. Mackensen (2001), How iceberg calving and grounding change the circulation and hydrography in the Filchner Ice shelf: Ocean system, *J. Geophys. Res.*, *106*, 9039–9055.

Holland, D. M., R. R. Rosales, D. Stefanica, and E. G. Tabak (2002), Internal hydraulic jumps and mixing in two-layer flows, *J. Fluid Mech.*, *470*, 63–83.

Killworth, P. D. (1977), Mixing on the Weddell Sea continental slope, *Deep Sea Res.*, *24*, 427–448.

Long, R. R. (1954), Some aspects of the flow of stratified fluids: II. Experiments with a two- fluid system, *Tellus*, *2*, 97–115.

Mensch, M., R. Bayer, J. L. Bullister, P. Schlosser, and R. F. Weiss (1997), The distribution of Tritium and CFCs in the Weddell Sea during the Mid 1980s, *Progr. Oceanogr.*, *38*, 377–414.

Mensch, M., W. M. Smethie Jr., P. Schlosser, R. Weppernig, and R. Bayer (1998), Transient tracer observations from the western Weddell Sea during the drift and recovery of Ice Station Weddell, *Antarctic Res. Ser.*, *75*, 241–256.

Middelton, J. H., T. D. Foster, and A. Foldvik (1982), Low-frequency currents and continental shelf waves in the Southern Weddell Sea, *J. Phys. Oceanogr.*, *12*, 618–634.

Middelton, J. H., T. D. Foster, and A. Foldvik (1987), Diurnal Shelf Waves in the Southern Weddell Sea, *J. Phys. Oceanogr.*, *17*, 784–791.

Millero, F. J. (1978), Freezing point of sea water, Eighth Report of the Joint Panel of Oceanographic Tables and Standards, Appendix 6, *UNESCO Tech. Pap. Mar. Sci.*, *28*, 29–31.

Muench, R. D., and A. L. Gordon (1995), Circulation and transport of water along the western Weddell Sea margin, *J. Geophys. Res.*, *100*, 18,503–18,515.

Naveira Garabato, A. C., E. L. McDonagh, D. P. Stevens, K. J. Heywood, and R. J. Sanders (2002), On the export of Antarctic Bottom water from the Weddell Sea, *Deep Sea Res.*, *49*, 4715–4742.

Nicholls, K. W., and S. Østerhus (2003), Interannual variability beneath Filchner - Ronne Ice Shelf, Antarctica, in *Filchner Ronne Ice Shelf Programme*, *Rep. 14*, edited by H. Oerter, Alfred-Wegener-Inst. for Polar and Marine Res, Bremerhaven, Germany.

Nicholls, K. W., S. Østerhus, K. Makinson, and M. R. Johnson (2001), Oceanographic conditions south of Berkner Island, beneath Filchner-Ronne Ice Shelf, Antarctica, *J. Geophys. Res.*, *106*, 481–492.

Nordlund, N. (1992), Bottom currents at the Continental slope in the Southern Weddell Sea (in Norwegian), Cand.Sci. thesis, Univ. of Bergen, Bergen.

Nøst, O. A., and S. Østerhus (1998), Impact of grounded icebergs on the hydrographic conditions near the Filchner Ice Shelf, in *Ocean, Ice and Atmosphere: Interactions at the Antarctic Continental Margin*, *Antarct. Res. Ser.*, vol. 75, edited by S. S. Jacobs, and R. F. Weiss, pp. 267–284, AGU, Washington, D. C.

Nygaard, E. (1994), Transport of ice shelf water in the Weddell Sea (in Norwegian), Can. Sci. thesis, Univ. of Bergen, Bergen.

Orsi, A. H., G. C. Johnson, and J. L. Bullister (1999), Circulation, mixing and production of Antarctic bottom water, *Prog. Oceanogr.*, *43*, 55–109.

Østerhus, S., and R. A. Krause (1990), Ausbringung und Bergung von ozeanographischen Verankerungen. Die Expedition ANTARKTIS-V mit FS "Polarstern" 1986/87, *Ber. zur Polarforschung*, *57*.

Padman, L., and C. Kottmeier (2000), High-frequency ice motion and divergence in the Weddell Sea, *J. Geophys. Res.*, *105*, 3379–3400.

Renfrew, I. A., J. C. King, and T. Markus (2002), Coastal polynyas in the southern Weddell Sea: Variability of the surface energy budget, *J. Geophys. Res.*, *107*(C6), 3063, doi:10.1029/2000JC000720.

Robertson, R., L. Padman, and G. D. Egbert (1998), Tides in the Weddell Sea, in *Ocean, Ice and Atmosphere: Interactions at the Antarctic Continental Margin*, *Antarct. Res. Ser.*, vol. 75, edited by S. S. Jacobs and R. F. Weiss, pp. 341–369, AGU, Washington, D. C.

Schlosser, P., R. Bayer, A. Foldvik, T. Gammelsrød, G. Rohardt, and K. O. Munnich (1990), Oxygen 18 and Helium as tracers of Ice Shelf Water and water/ice interaction in the Weddell Sea, *J. Geophys. Res.*, *95*, 3253–3263.

Tanaka, K., and K. Akitomo (2001), Baroclinic instability of density current along a sloping bottom and the associated transport process, *J. Geophys. Res.*, *106*, 2621–2638.

United Nations Educational, Scientific and Cultural Organization (UNESCO) (1981), The Practical Salinity Scale 1978 and the International Equation of State of Seawater 1980, *Unesco Tech. Pap. Mar.*, *36*.

Weiss, R. F., H. G. Østlund, and H. Craig (1979), Geochemical studies in the Weddell Sea, *Deep Sea Res.*, *26A*, 1093–1120.

Weppernig, R., P. Schlosser, S. Khatiwala, and R. G. Fairbanks (1996), Isotope data from Ice Station Weddell: Implications for deep water formation in the Weddell Sea, *J. Geophys. Res.*, *101*, 25,723–25,739.

Woodgate, R. A., M. Schröder, and S. Østerhus (1998), Moorings from the Filchner trough and the Ronne Ice Shelf Front: Preliminary Results, in *Filchner Ronne Ice Shelf Programme*, 12, edited by H. Oerter, pp. 85–90, Alfred-Wegener-Inst. for Polar and Mar. Res, Bremerhaven, Germany.

E. Fahrbach, G. Rohardt, and M. Schröder, Alfred-Wegener-Institut fur Polar und Meeresforschung, Postfach 120162, 27512, Bremerhaven, Germany.

A. Foldvik, T. Gammelsrød, and S. Østerhus, Geophysical Institute, University of Bergen, 5008 Bergen, Norway. (arne.foldvik@uib.no)

K. W. Nicholls, British Antarctic Survey, High Cross, Madingley Road, Cambridge CB3 0ET, UK.

L. Padman, Earth and Space Research, 1910 Fairview Avenue East, Suite 210, Seattle, WA 98102, USA.

R. A. Woodgate, Applied Physics Laboratory, University of Washington, 1013 NE 40th Street, Seattle, WA 98105, USA.